Distribution behaviour of B and P in Si-slag system at 1500 °C

K. Avarmaa[1], A. Putera[2], J. Chen[3], G. Brooks[4], M. A. Rhamdhani[5*]*

1. Postdoctoral Research Fellow, Fluid and Process Dynamics (FPD) Research Group, Swinburne University of Technology, Melbourne, VIC, 3122, Australia. Email: kavarmaa@swin.edu.au
2. PhD Student, Fluid and Process Dynamics (FPD) Research Group, Swinburne University of Technology, Melbourne, VIC, 3122, Australia. Email: aputera@swin.edu.au
3. Researcher, School of Chemical Engineering, The University of Queensland, Brisbane, Queensland, 4072, Australia. Email: jcanu2018@gmail.com
4. Professor, Fluid and Process Dynamics (FPD) Research Group, Swinburne University of Technology, Melbourne, VIC, 3122, Australia. Email: gbrooks@swin.edu.au
5. Professor, Fluid and Process Dynamics (FPD) Research Group, Swinburne University of Technology, Melbourne, VIC, 3122, Australia. Email: arhamdhani@swin.edu.au

*Corresponding authors

Keywords: Slag treatment, Si refining, PV cell recycling, phase equilibrium, LA-ICP-MS

ABSTRACT

Silicon-based photovoltaic cells are currently the most dominant types applied to convert solar energy to electricity. In solar-grade silicon (SG-Si), the control of boron (B) and phosphorus (P) is very critical. Generally, these elements are difficult to remove into acceptable sub-ppm levels from lower grade Si. This study investigates slag treatment as a process for Si refining, focussing on the behaviour of P and B. The experiments were conducted by equilibrating Si-B-P alloys with 43 wt.% SiO_2–47 wt.% CaO–10 wt.% Al_2O_3 slag under inert atmosphere at 1500 °C. Different crucible materials were used (Al_2O_3, SiO_2 and MgO), which determined the primary saturation phase for the system and modified the final slag composition accordingly. The samples were equilibrated and analysed with microanalysis techniques (EPMA and LA-ICP-MS). New standards were prepared and applied in the LA-ICP-MS analyses. Experimental results show that silver is essentially fully dissolved in silicon, as well as most phosphorus with L_P (=wt.% P in slag / wt.% P in Si) between 0.1–0.3. The distribution coefficient of boron was measured to be between 1 and 2. The crucible material used had an influence on the phase compositions and slight influence on the distribution coefficients of boron and phosphorus. The experimental results provided new accurate data when considering applicability of slag treatment as a technique for Si refining and Si PV cell recycling.

INTRODUCTION

Boron and phosphorus naturally occur in the ore deposits used for silicon and ferrosilicon production. Their removal is very challenging and metallurgical grade silicon (>98 wt.% purity) produced in electric arc furnace need to be refined via complex and energy-intensive Siemens process (>200 kWh/kg, (Braga *et al.*, 2008; Chigondo, 2018) into higher purity solar grade silicon (>99.99 wt.%). Potential secondary Si include various Si scraps, such as kerf slurry and end-of-life Si PV cells. These materials contain varying concentrations of B and P (a few ppm to thousands of ppm) (Chen *et al.*, 2019; Yang *et al.*, 2019; Liu, Huang and Zhu, 2017). Silver do not naturally occur in the silicon ore resources but exist in high concentrations end-of-life silicon PV cells, ~500-8000 ppmwt (Latunussa *et al.*, 2016, Wang *et al.*, 2022).

Different technologies for refining MG-Si and Si scraps have been investigated and proposed, such as slag treatment (Chigondo, 2018) and electrically-enhanced slag treatment (Wang *et al.*, 2018; Islam, Rhamdhani and Brooks, 2014. Several studies investigating boron distribution behaviour in Si-slag systems can be found from the literature, but very limited is available for phosphorus. There exist various types of slags investigated for boron removal from molten silicon or silicon alloy, such as CaO-SiO_2/MgO, CaO-SiO_2-Al_2O_3/MgO/CaF_2/TiO_2/BaO/Na_2O/LiF/Li_2O and CaO-SiO_2-Al_2O_3-MgO (Chen *et al.*, 2018; Jung, Moon and Min, 2011; Zhou *et al.*, 2019). Table 1 presents the best comparable studies (limited to CaO-SiO_2-Al_2O_3-MgO slags) conducted to study boron and phosphorus distribution behaviour between molten silicon and slag.

TABLE 1 – Literature on B and P distribution behaviour in Si alloy- slag systems.

Elements	Si alloy	Slag	Conditions	Result	Reference
B	Si	$CaO-SiO_2$, $CaO-SiO_2-Al_2O_3$	1450–1600 °C, Al_2O_3 cru, 4 g (slag/Si:1–3), t: 0-4 h, Ar	L_B: 1.6-3.2	Islam, 2015.
B	MG-Si	$CaO-SiO_2$-LiF/Li_2O	1550 °C, gr. cru, 70 g slag (slag/Si:0.5-5), t:0–4 h, Ar	L_B=1 for $CaO-SiO_2$, for Li-containing L_B= 1.2–2.8	Ding *et al.,* 2012
B	Si	SiO_2-CaO/MgO, SiO_2-CaO-MgO/Al_2O_3	1600 °C, gr. cru, 30 g (slag/Si:1), t:0–9 h, Ar	L_B=2–2.5, for high alumina L_B=1.3	Jakobsson and Tangstad, 2018; 2014
B	Si	$CaO-SiO_2$-Al_2O_3/CaF2/MgO/BaO	1600 °C, Al_2O_3 cru, t:0–5 h, Ar	L_B=0.35–1.1	Fujiwara *et al.,* 1996 (in Japanese)
B	Si	$CaO-SiO_2$	1550 °C, gr. cru, 9.7 g (slag/Si:2.2), t: 18 h, Ar	L_B=2–5	Teixeira *et al.*, 2009
B	Si	$CaO-SiO_2$	1550 °C, gr. cru, 4 g slag (slag/Si:0.4-0.8), t:0–3h, Ar or Ar-Cl_2	L_B=2-2.2 (under Ar and Ar-Cl_2)	Nishimoto *et al.*, 2012
B	Si	$CaO-SiO_2$/-MgO/BaO/CaF_2	1450–1550 °C, gr. cru, 20 g (slag/Si: 2), 2 h, CO, Ar or Ar-CO_2	L_B=0.4–2, T and CaO concentration in slag increased L_B	Suzuki and Sano, 1991
B	Si	SiO_2-CaO	1500 °C, SiO_2 cru, t:4–6.5 h, Ar	L_B=1.7	Weiss and Schwerdtfeger, 1994
B	Si	SiO_2-CaO/-Al_2O_3/Na_2O/CaF_2	1450–1600 °C, quartz ceramic cru, 3.3 kg (slag/Si:10), 0.5–2 h, Ar	L_B=2–9	Luo *et al.*, 2011
B	Si-20 wt.% Fe	$CaO-SiO_2-Al_2O_3$	1600 °C, Al_2O_3 cru., 10 g (slag/Si:1), 8 h, Ar	L_B=1–11 (mainly around 1-2)	Hosseinpour and Khajavi, 2018
B	Si-Fe (0-85 wt.% Fe)	$CaO-SiO_2$-CaO	1600 °C, gr. cru, 8–11 g (slag/Si:1, slag/Si-Fe:0.6), t:0–4 h, Ar	L_B=2 (up to 75 wt.% Fe in Si), 6 for 85 wt.% Fe in Si	Krystad *et al.*, 2017
B	Si kerf / Si kerf ceramics	SiO_2-CaO/-CaF_2	gr. cru, 50 g (slag/Si kerf:1), 40 min	L_B=2.8–6.8 depending on optical basicity and CaF_2	Zhang *et al.*, 2020
B	Mg-Si	$CaO-SiO_2$	1550 °C, gr. cru, 140 g (slag/Si:1), 0.5–3 h, Ar	L_B=0.7–1.6 depending on optical basicity	Wei *et al.*, 2015
B, P	Mg-Si	$CaO-SiO_2-Al_2O_3$-MgO, Al_2O_3-SiO_2-BaO	1500 °C, MgO / Al_2O_3 cru, 13 g (slag/Si:1.4), t:0–6 h, Ar	L_B=1–2, L_P=0.1–0.4 at Al_2O_3-sat, L_P=1–9 at MgO-sat (when SiO_2/Al_2O_3 >1)	Johnston and Barati, 2010
P	Si-20 wt.% Fe	$CaO-SiO_2-Al_2O_3$/-Na_2O	1300 °C, Al_2O_3 cru, 10 g (slag/Si-Fe:1), t:2–10 h, Ar	L_P=0.2-1.2 (Na_2O, CaO/SiO_2 and SiO_2/Al_2O_3 increased L_P)	Taposhe and Khajavi, 2021
P	Si(-Al-Ca)	$CaO-SiO_2-Al_2O_3$.	1600 °C, Al_2O_3 cru, 6–9.5 g (slag/Si:2), 5 h, Ar	L_P=0.01–3 ($CaO/(CaO+SiO_2)$ increased L_P)	Fujiwara *et al.*, 1996
P	Si-20 wt.% Fe	$CaO-SiO_2-Al_2O_3$	1600 °C, Al_2O_3 cru., 10 g (slag/Si:1), 8 h, Ar	L_P=0.01-0.2	Hosseinpour and Khajavi, 2019

Overall, the results on the influence of slag treatment on the boron and phosphorus removal from molten silicon are not clear and vary between different studies as shown in Table 1. All the previous studies have used 5-30 g sample primary chemical bulk analyses that can increase the risk of distorted results due to entrained phase droplets within wrong phase analysis. This study investigated the distribution behaviour of B and P between molten silicon and SiO_2-CaO-Al_2O_3/-MgO slags at 1500 °C by using experimental technique of drop-quenching followed by microanalyses.

EXPERIMENTAL

The drop-quenching technique followed by microanalyses has been used in great extent for equilibrium studies and on minor element investigations in copper and nickel smelting conditions (Chet *et al.*, 2022; Piskunen *et al.*, 2018; Sineva *et al.*, 2021 and 2023). It enables to measure in-situ ppmwt or even ppbwt concentration of elements in different phases and without risk of having entrapped 'wrong' phase distorting the analysis results, as can occur in bulk chemical analyses.

Materials

Si-P-B master alloys, as well as SiO_2-CaO-Al_2O_3 master slag were prepared for the experiments. The reagent materials were high-purity powders (99.9 % or above) supplied by Merck Life Science Pty Ltd and Thermo Fisher Scientific Australia Pty Ltd. Si-P-B powder mixtures were weighted into BN-painted alumina crucible and melted for 2 h in a vertical tube furnace under Ar gas atmosphere at 1500 °C. The master slag was mixed into homogeneous powder mixture, melted in Pt crucible for 1 h in a muffle furnace and cast to a steel rail. The final compositions of the master alloys and slag measured by ICP-AES and SEM-EDS are presented in Table 2.

TABLE 2 – Si master alloy compositions by ICP-AES and normalized slag composition results by ICP-AES and SEM-EDS.

Si master alloys	**B / ppm wt**	**P / ppm wt**	**Ag / ppm wt**	**Al / ppm wt**	**Ca / ppm wt**
Si-P-B	570	150		685	320
Slag	**CaO / wt.%**	**SiO_2 / wt.%**	**Al_2O_3 / wt.%**		
ICP-AES	47.1	43.2	9.7		
SEM-EDS	45.6	44.0	10.4		

As a new experimental technique for silicon-slag systems, appropriate standards for LA-ICP-MS analyses were prepared for silicon. Silicon standards were melted in alumina crucibles under Ar at 1500 °C and drop-quenched into ice water. The final compositions of the standards are presented in Table 3.

TABLE 3 – Si standard compositions measured by ICP-AES.

	B / ppm wt	**P / ppm wt**	**Ag / ppm wt**	**Al / ppm wt**	**Ca / ppm wt**
S1	555	845	1260	1780	30
S2	540	1540		1980	35
S3	720	165		1310	45

Three different crucibles were used in the experiments; Al_2O_3 (99.53 %), SiO_2 (99.99 %) and MgO (97.18 %) all supplied by Nanyang Yaki, China. The used crucible material will define the primary phase field of the system and slag composition will change accordingly.

Experiments

The experiments were carried out in a vertical tube furnace Nabertherm RHTV 120-300/18 and Nabertherm controller unit C42. The furnace temperature was measured with a calibrated B-type thermocouple (TC Measurement & Control Pty Ltd, Australia) inserted next to the sample and the followed through the experiment by using digital thermometer Anzeiger 32h8i (Eurotherm controller 32h8). The schematics of the experimental assembly is presented in Figure 1.

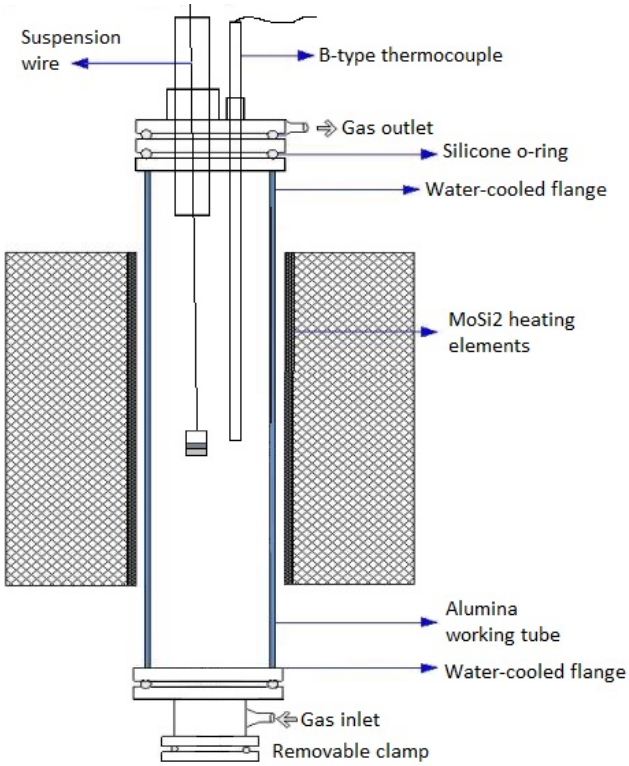

FIGURE 1 – Experimental apparatus.

First 0.2 g of master Si alloy and 0.4 g of master slag were measured in a crucible (initial slag/Si ratio = 2). A CaO-SiO_2-Al_2O_3 slag system was used in the study as this resembles a typical slag in the blast furnace iron making. The crucible was attached to the suspension wire which was a combination of Kanthal A1 and Mo or Pt wires. The hot zone of the furnace was measured at 1500 °C, and the suspension wire combo was carefully measured for each experiment to be assure that the sample was in the hot zone during the experiment. The crucible attached to the suspension wire was first lowered into the guiding tube, that was large enough to fit the crucible through it and kept in the cold zone for 30 min while Ar gas atmosphere was created. Argon flow was controlled with a mass-flow controller (Aalborg DFC26, USA; accuracy ±1 pct) and set to flow rate of 200 ml/min. After 30 min, the sample was lowered to the hot zone and the experiment started. After required time was full, the sample was drop-quenched into an ice water bucket. Time series to determine the equilibration times required at each crucible was conducted. The system was considered to reach the equilibrium when the slag composition was stabilized and homogenous throughout the sample. It was found that equilibration time of 8h was enough for the Si-B-P alloy equilibrated with slag at silica-saturation at 1500 °C; while 16h equilibration time was enough for the Si-B-P alloy equilibrated with slag at alumina-saturation and magnesia-saturation at 1500 °C.

Analytical techniques

Samples were mounted into epoxy resin and their cross-sections were prepared for microanalyses by using traditional wet-metallographic techniques and imaged by optical microscope. The microanalyses included electron microprobe analysis and laser ablation inductively coupled plasma mass spectrometer measurements.

Microstructure examination and quantitative elemental analysis were performed on the experimental samples using a JEOL 8530F Plus field-emission electron microprobe at the Centre for Advanced

Microscopy, Australian National University. For the major elements (> 0.5 m-%), an acceleration voltage of 15 keV and a probe current of 40 nA were used; for the minor and trace elements (< 0.5 wt.%), a probe current of 1000 nA were used. A probe size of 50–100 µm was chosen for slag and alloy phase. A list of elements, their emission lines analysed and the minimum detection limited are given in Table 4.

TABLE 4 – List of elements, their emission lines analysed and the minimum detection limit by EPMA.

Slag	**Ca**	**Mg**	**Al**	**Si**	**Y**	**Zr**	**P**
Emission line	Kα	Kα	Kα	Kα	Lα	Lα	Kα 2nd order
Detection limit (ppm wt)	60	50	100	120	60	80	10–15
Si alloy	**Al**	**P**	**Ca**	**Mo**	**Zr**	**Fe**	**Ag**
Emission line	Kα	Kα	Kα	Lα	Lα	Kα	Lα
Detection limit (ppm wt)	12	15	5	16	25	12	55

Trace elements in the samples collected were determined by LA-ICP-MS at the Research School of Earth Sciences, ANU using an Agilent Technologies 7700 ICP-MS coupled to an ANU HelEX laser-ablation system with a 193-nm-wavelength EXCIMER laser (110 (ArF) COMPex, Lambda Physik). The elements determined and the isotopes used for these determinations were ^{11}B, ^{26}Mg, ^{27}Al, ^{31}P, ^{43}Ca, ^{57}Fe, ^{89}Y, ^{90}Zr, ^{95}Mo and ^{107}Ag. Data acquisition involved a 15 s background measurement followed by 30 s of ablation, with a 7 Hz repetition rate. The laser spot size was set to 81 µm. For the slag phase, NIST SRM 612 was used as the external reference standard and NIST SRM 610 was used for quality control standard; for the Si alloy phase, three Si alloy standards made-in-house doped with different levels of B, P and Ag were used as both external and quality control standards. Si concentrations in the slag and alloy determined by EPMA were used as internal standards. Data were processed and quantified using the Iolite v4 software package. The minimum detection limits for the elements analysed are given in Table 5.

TABLE 5 – Minimum detection limits for the elements analysed by LA-ICP-MS.

	B	**Mg**	**Al**	**P**	**Ca**
Slag (ppm wt)	0.2–0 .6	1–7	1–10	0.9–2	-
Alloy (ppm wt)	0.3–0.6	-	0.2–10	1–4	0.4–1
	Fe	**Y**	**Zr**	**Mo**	**Ag**
Slag (ppm wt)	0.5–1.5	0.003–0.05	0.01–0.1	0.01–0.05	0.01–0.03
Alloy (ppm wt)	10–40	-	-	-	0.05–1.5

RESULTS AND DISCUSSION

The equilibrated samples involved and discussed in this study are:

- Si-B-P – SiO_2-CaO-Al_2O_3 slag at silica-saturation at 1500 °C equilibrated 8 h
- Si-B-P – SiO_2-CaO-Al_2O_3 slag at alumina-saturation at 1500 °C equilibrated 16 h
- Si-B-P – SiO_2-CaO-Al_2O_3 slag at magnesia-saturation at 1500 °C equilibrated 16 h

Backscatter images of the samples at different saturations, as well as an optical microscope image of the cross-section of the alumina-saturated system is shown in Figure 2.

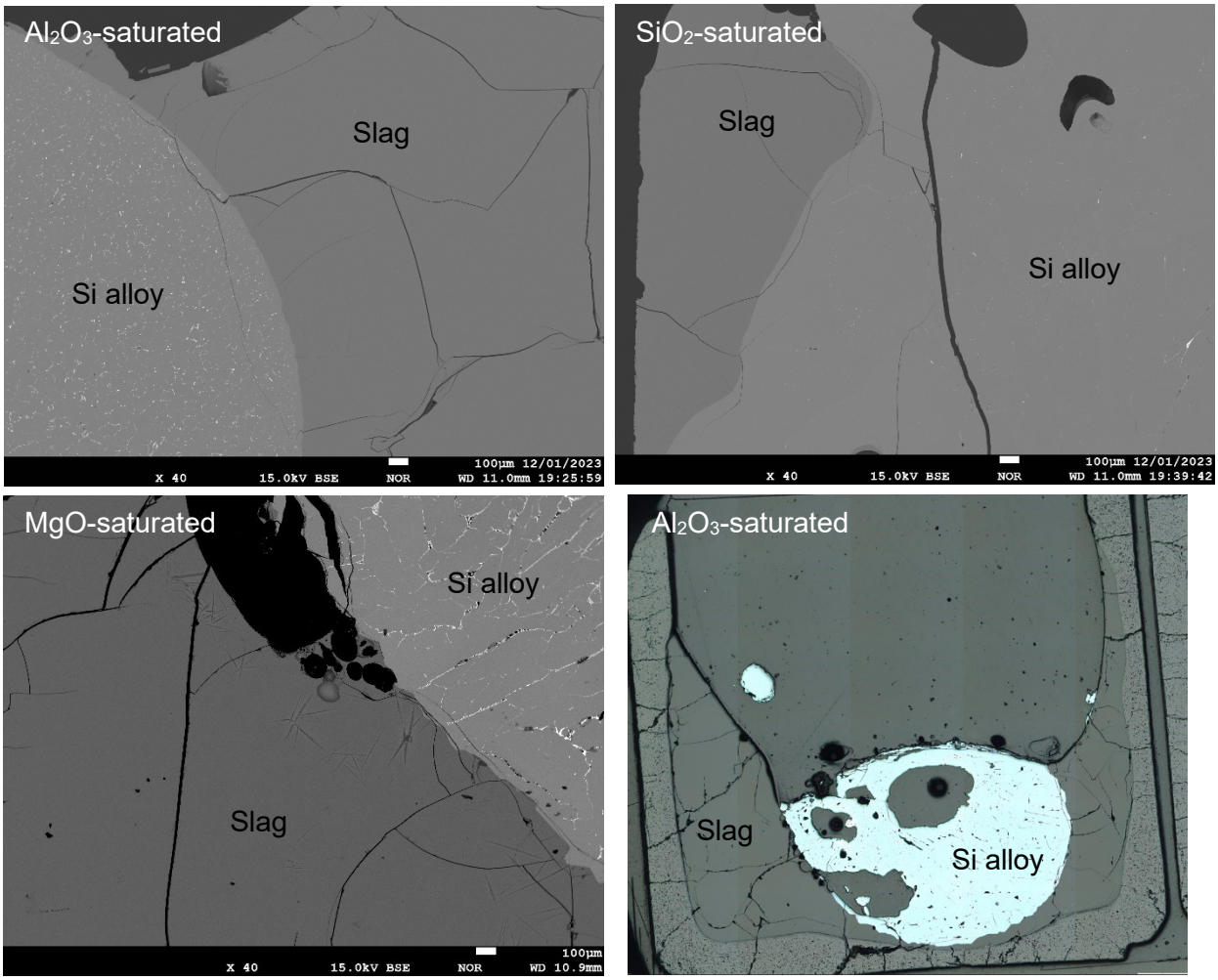

FIGURE 2 – BSE-images of the samples at different saturations and an optical microscope image of the cross-section of the alumina-saturated sample.

As shown in Figure 2, slag phase was quenched well and formed a homogeneous phase, whereas Si alloy had bright segregations, especially at alumina and magnesia-saturated systems (most likely caused by primary precipitations of Si intermetallics). As the brighter segregations are part of the Si alloy, the beam sizes of microanalyses were chosen larger to evaluate the overall phase composition. Nevertheless, this heterogeneity of the phase caused discrepancy within the taken Si alloy analyses causing in some cases rather high standard deviations for certain elements. Some needle formations were visible in slag phase in MgO-saturated samples that were excluded from the analyses. Slag analyses were taken from homogeneous slag areas and close to Si alloy. The Si alloy was typically as a droplet formation on the top and middle of the slag as shown in the cross-section in Figure 2. Molten silicon has somewhat lower density when compared to the used slags that explains the behaviour. Literature (Krystad *et al.* and Zhou *et al.* 2019) presents that Si and Si-rich alloys (up to 75 % Fe) formed a droplet in the middle of the crucible and on top of slag similarly as in our study. The final slag compositions for main components are presented in Table 6. Traces of Zr, Y and Mg (30–90 ppmwt) were also measured in the slags. The final compositions are clearly different to the initial slag composition presented in Table 2. Each have dissolved crucible material, and the equilibrium slag compositions present the tie line conditions for the slag-primary phase field at 1500 °C.

TABLE 6 – The slag compositions of equilibrated samples, in wt pct.

	CaO	SiO_2	Al_2O_3	MgO	Y_2O_3
Silica-saturated	27.7	66.8	5.5		
Alumina-saturated (P, B)	29.4	26.0	44.3		0.3
Alumina-saturated (Ag)	28.5	27.6	43.6		0.3
Magnesia-saturated	22.9	40.0	12.4	24.6	0.2

Phosphorus concentration was measured by EPMA and LA-ICP-MS techniques in both phases of interest. The comparison of EPMA and LA-ICP-MS results for P in slag is shown in Figure 3 and for Si alloy in Figure 4. EPMA results for phosphorus in slag at MgO and Al_2O_3-saturations were somewhat higher than measured by LA-ICP-MS, but relatively well in agreement. Si alloy phase with its segregations (i.e. heterogeneous phase structure), and lack of known standards for Si alloy required by LA-ICP-MS, made the measurements challenging. LA-ICP-MS results are extrapolated in relation to the standard used, and as the standard 1 (S1) included much higher P concentration than expected in the samples, the measured value might be exaggerated upwards. As can be noticed S1 gave clearly higher values than EPMA and LA-ICP-MS with S3, thus the results by S1 can be ruled out. When comparing the measured P concentrations in Si between EPMA and LA-ICP-MS with S3, alumina and magnesia-saturated system had a noticeable difference. This can be partially or fully related to the heterogeneous Si phase structure, whereas for more homogeneous Si alloy at silica-saturated system, EPMA and LA-ICP-MS provided better fit.

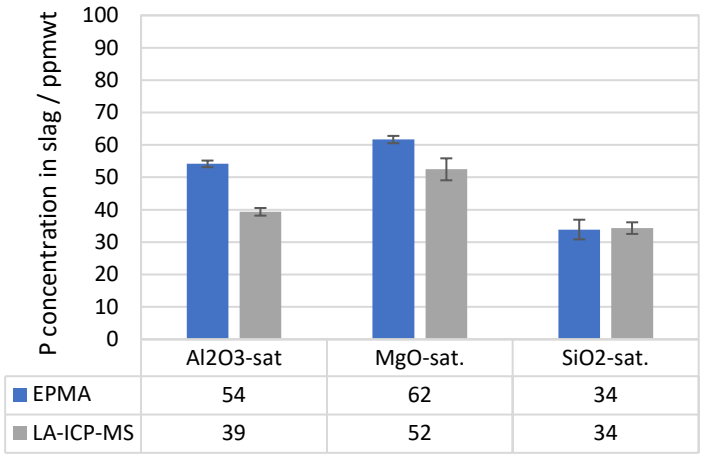

FIGURE 3 – Phosphorus concentration in slag measured by EPMA and LA-ICP-MS at different saturation phases at 1500 °C.

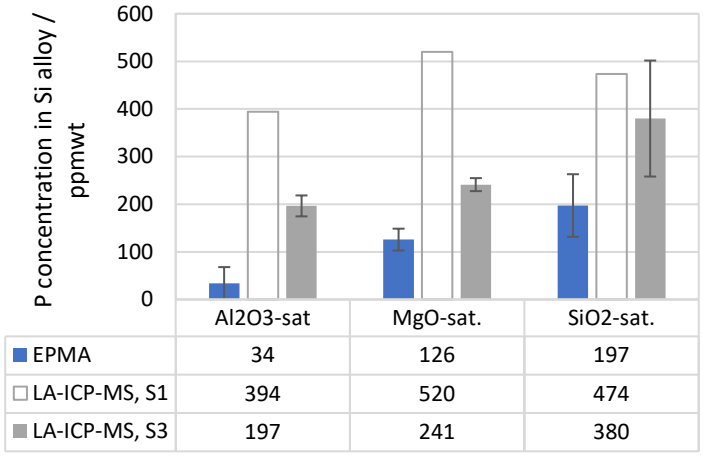

FIGURE 4 – Phosphorus concentration in Si alloy measured by EPMA and LA-ICP-MS (two different standards) at different saturation phases at 1500 °C.

Boron was measured only by LA-ICP-MS technique and the results are presented in Figure 5 and Figure 6 for slag and Si alloy, respectively. Boron concentration was radically higher in both phases in MgO-saturated system when compared to silica and alumina-saturated systems, even though the used master Si alloy and master slag were same for all systems. Possibly MgO-crucible contained boron as an impurity and thus had higher concentration in the system. Another reason might be that MgO-slag might retain boron from vaporization more compared to other systems investigated. Both standards S1 and S3 provided rather similar results for B in Si alloy, which can be expected as they have rather similar concentrations in the used standards.

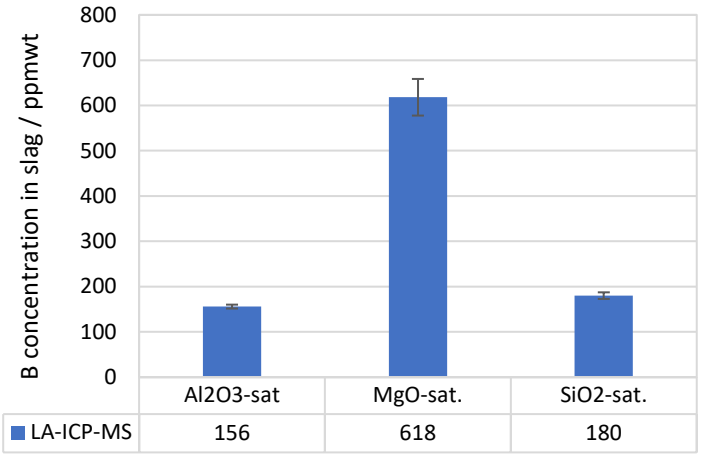

FIGURE 5 – Boron concentration in slag measured by LA-ICP-MS at different saturation phases at 1500 °C.

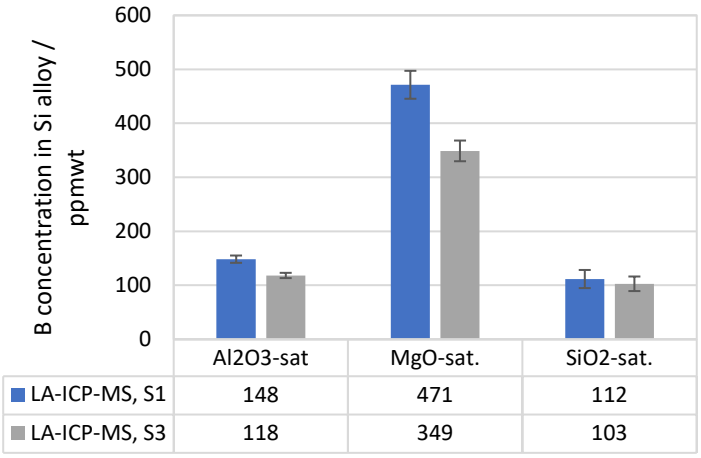

FIGURE 6 – Boron concentration in Si alloy measured by LA-ICP-MS (two different standards) at different saturation phases at 1500 °C.

The distribution coefficient of element is determined as:

$$L_M = (M)_{\text{in slag}} / [M]_{\text{in Si alloy}} \quad (1)$$

When considering minor element behaviour in molten Si - slag system, the distribution behaviour relates to its oxidation reaction as follows:

$$[M] + x/2\ O_2 = (x\ MO_2) \quad (2)$$

or

$$[M] + (SiO_2) = [Si] + (MO_2) \quad (3)$$

By employing the equilibrium constant of the reaction (2), the distribution coefficient of element can be defined thermodynamically as follows:

$$K = \frac{a_{MO_X}}{a_M p_{O_2}^{x/2}} = \frac{\gamma_{MO_x}(m-\%M)/\cancel{M_M}(n_T)}{\gamma_M[m-\%M]/\cancel{M_M}[n_T]p_{O_2}^{x/2}} \quad (4)$$

$$\rightarrow L_M = \frac{(m-\%M)_{slag}}{[m-\%M]_{silicon}} = \frac{K[n_T]\gamma_M^o p_{O_2}^{x/2}}{(n_T)\gamma_{MO_x}} \quad (5)$$

When minor element exists in dilute form in silicon, it can be estimated to follow Henry´s law, *i.e.*, $\gamma_M^o \sim constant$. Additionally, the total number of moles (n_T) per 100 g of each phase can be considered constant when slag is presented in mono-cationic form. If the partial pressure of oxygen is known and the L_M, the activity coefficient of oxidic minor element can be evaluated. Other approach is via reaction (3) to evaluate the properties of the system and the minor element. Figures 8 and 9 presents the distribution coefficient of boron and phosphorus, respectively. L_B was calculated using results by both standards (S1 and S3), whereas L_P by using LA-ICP-MS results for Si alloy (S3), while EPMA and LA-ICP-MS results for slag phase.

Some differences depending on the technique and standard can be seen for alumina- and magnesia-saturated systems, that mainly can be explained by the heterogeneous Si alloy microstructure. Nevertheless, they still fit quite well with each other. Silica-saturate system had even more consistent results independent on the analysis technique or standard (more homogeneous Si alloy). Silica- and magnesia-saturated systems provided the highest L_B that indicates higher removal rate for boron between these three systems. Phosphorus was systematically distributed more on the silicon alloy, but the silica-saturated system provided the least favourable conditions for phosphorus removal.

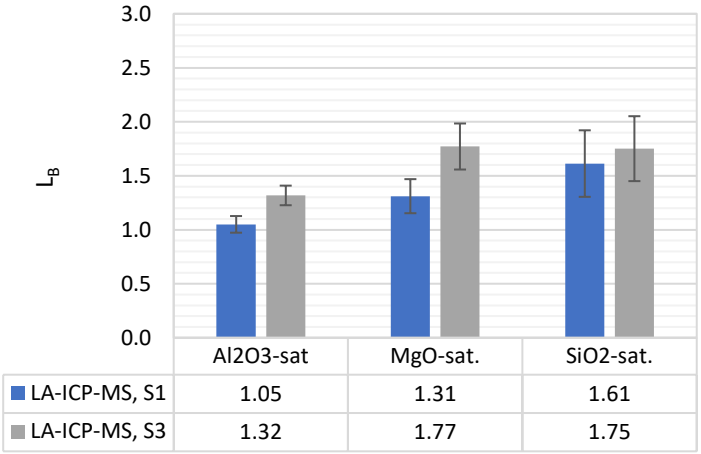

FIGURE 8 – Distribution coefficient of boron at different saturation phases at 1500 °C by LA-ICP-MS (two different standards).

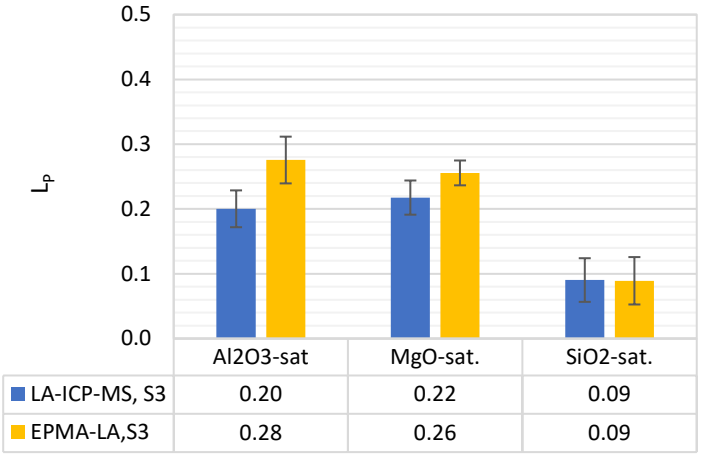

FIGURE 9 – Distribution coefficient of phosphorus at different saturation phases at 1500 °C by EPMA and LA-ICP-MS.

When comparing measured L_B results to the literature, they are similar results by various studies (Ding *et al.*, 2012; Jakobsson and Tangstad, 2018; Johnston and Barati, 2010; Suzuki and Sano, 1991; Weiss and Schwerdtfeger, 1994). Nevertheless, many studies have measured higher L_B values between 2–5 (Islam, 2015; Luo *et al.*, 2011; Teixeira *et al.*, 2009, Nishimoto *et al.*, 2012; Zhang *et al.*, 2020), and even up to 10 (Luo *et al.*, 2011; Hosseinpour and Khajavi, 2018). The investigated systems, experimental conditions (T, slag composition, crucible material) and techniques have varied in literature that have influenced more or less the results. In this study, the slag composition did not seem to have a major impact on the L_B. Similar conclusion was presented *e.g.*, the study by Jakobsson and Tangstad (2014). Most of the studies conducted for phosphorus, even with different type of slags and Fe-Si alloy provided distribution coefficients in the same range with our results (Fujiwara *et al.*, 1996; Hosseinpour and Khajavi, 2019; Johnston and Barati, 2010; Taposhe and Khajavi, 2021).

CONCLUSIONS

This study investigated the behaviour of B and P in molten Si alloy and slag systems under different saturations at 1500 °C. Experimental technique of drop-quenching followed by microanalyses; EPMA and LA-ICP-MS, were used for the first time to measure the minor element concentrations Si alloy and slag phases. Phosphorus and silver results by EPMA and LA-ICP-MS techniques were compared and discussed. Both techniques were applicable for phosphorus measurements. The distribution coefficients of P and B were not influenced radically by the slag composition and the crucible material, L_P varied between 0.1–0.3 and L_B between 1–2.

ACKNOWLEDGEMENTS

The authors are grateful to Australia Renewable Energy Agency (ARENA), Grant number 2020RND011. Additionally, Mr. Andreas Putera is grateful on the Swinburne University SUPRA PhD Scholarship. The authors acknowledge the help of Mr. Aidan O'Keeffe, the manager of Swinburne workshop (Fabrication and laboratory).

REFERENCES

Braga, A, Moreira, S, Zampieri, P, Bacchin, J and Mei, P, 2008. New processes for the production of solar-grade polycrystalline silicon: A review. *Solar energy materials and solar cells*, 92(4):418–424.

Chen, H, Morita, K, Ma, X, Chen, Z and Wang, Y, 2019. Boron removal for solar-grade silicon production by metallurgical route: A review. Solar Energy Materials and Solar Cells, 203, 110169.

Chen, J, Fallah-Mehrjardi, A, Specht, A and O'Neill, H, 2022. Measurement of minor element distributions in complex copper converting slags using quantitative microanalysis techniques. *JOM* 74:185–194.

Chigondo, F, 2018. From metallurgical-grade to solar-grade silicon: an overview. *Silicon*, 10:789–798.

Fujiwara, H, Liang, J, Takeuchi, K and Ichise, E, 1996. Reducing removal of phosphorous from calcium containing silicon alloys. *Materials transactions, JIM*, 37(4):923–926.

Hosseinpour, A and Khajavi, L, 2019. Phosphorus Removal from Si-Fe Alloy Using SiO_2-Al_2O_3-CaO Slag. *Metallurgical and Materials Transactions B*, 50:1773–1781.
Hosseinpour, A and Khajavi, L, 2018. Thermodynamics of boron removal in slag refining of Fe-Si alloy. *Journal of Alloys and Compounds*, 768:545–552.
Islam, M, 2015. Electrically Enhanced Slag-Metal Reactions. Doctoral Thesis, Swinburne University of Technology, 242 pp.
Islam, M, Rhamdhani, M and Brooks, G, 2014. Electrically enhanced boron removal from silicon using slag. *Metallurgical and Materials Transactions B*, 45:1–5.
Jakobsson, L and Tangstad, M, 2018. Thermodynamics of Boron Removal from Silicon Using CaO-MgO-Al_2O_3-SiO_2 Slags. *Metallurgical and Materials Transactions B*, 49:1699–1708.
Jakobsson, L and Tangstad, M, 2014. Distribution of boron between silicon and CaO-MgO-Al_2O_3-SiO_2 slags. *Metallurgical and Materials Transactions B*, 45:1644–1655.
Johnston, M and Barati, M, 2010. Distribution of impurity elements in slag–silicon equilibria for oxidative refining of metallurgical silicon for solar cell applications. *Solar energy materials and solar cells*, 94(12):2085–2090.
Jung, E, Moon, B and Min, D, 2011. Quantitative evaluation for effective removal of phosphorus for SoG-Si. *Solar energy materials and solar cells*, 95(7):1779–1784.
Krystad, E, Jakobsson, L, Tang, K and Tranell, G, 2017. Thermodynamic behavior and mass transfer kinetics of boron between ferrosilicon and CaO-SiO_2 slag. *Metallurgical and Materials Transactions B*, 48:2574–2582.
Latunussa, C, Ardente, F, Blengini, G and Mancini, L, 2016. Life Cycle Assessment of an innovative recycling process for crystalline silicon photovoltaic panels. *Solar energy materials and solar cells*, 156:101–111.
Liu, S, Huang, K and Zhu, H, 2017. Source of boron and phosphorus impurities in the silicon wiresawing slurry and their removal by acid leaching. *Separation and Purification Technology*, 172:113–118.
Piskunen, P, Avarmaa, K, O'brien, H, Klemettinen, L, Johto, H and Taskinen, P, 2018. Precious metal distributions in direct nickel matte smelting with low-Cu mattes. *Metallurgical and Materials Transactions B*, 49:98–112.
Sineva, S., Shishin, D., Prostakova, V., Lindgren, M., Starykh, R., Chen, J., Jak, E. "Experimental Study and Thermodynamic Modelling of Equilibrium Distributions of Ni, Sn and Zn Between Slag and Black Copper for E-Scrap Recycling Applications" (2023) JOM, 75 (10), pp. 4254-4268
Sineva, S., Shishin, D., Starykh, R., Hayes, P.C., Jak, E. "Equilibrium Distributions of Pb, Bi, and Ag between Fayalite Slag and Copper-Rich Metal, Calcium Ferrite Slag and Copper-Rich Metal. Thermodynamic Assessment and Experimental Study at 1250 °C" (2021) Journal of Sustainable Metallurgy, 7 (2), pp. 569-582
Suzuki, K and Sano, N, 1991. Thermodynamics for removal of boron from metallurgical silicon by flux treatment. In Tenth EC Photovoltaic Solar Energy Conference: Proceedings of the International Conference, held at Lisbon, Portugal, 8–12 April 1991 (pp. 273-275). Dordrecht: Springer Netherlands.
Wang, Z, Ge, Z, Liu, J, Qian, G and Du, B, 2018. The mechanism of boron removal from silicon alloy by electric field using slag treatment. *Separation and Purification Technology*, 199:134–139.
Wang, X, Tian, X, Chen, X, Ren, L and Geng, C, 2022. A review of end-of-life crystalline silicon solar photovoltaic panel recycling technology. *Solar Energy Materials and Solar Cells*, 248, 111976.
Wei, K, Lu, H, Ma, W, Li, Y, Ding, Z, Wu, J and Dai, Y, 2015. Boron removal from metallurgical-grade silicon by CaO–SiO_2 slag refining. *Rare Metals*, 34:522–526.
Weiss, T and Schwerdtfeger, K, 1994. Chemical equilibria between silicon and slag melts. *Metallurgical and materials transactions B*, 25:497–504.
Yang, H, Liu, I, Liu, C, Hsu, H and Lan, C, 2019. Recycling and reuse of kerf-loss silicon from diamond wire sawing for photovoltaic industry. *Waste Management*, 84:204–210.
Zhang, Y, Sheng, W, Huang, L, Zhang, S, Chen, G, Zhang, C, Cai, H, Meng, J and Luo, X, 2020. Preparation of low-boron silicon from diamond wire sawing waste by pressure-less sintering and CaO–SiO2 slag treatment. *ACS Sustainable Chemistry & Engineering*, 8(31):11755–11763.
Zhou, Q, Wen, J, Wu, J, Ma, W, Xu, M, Wei, K, Zhang, Z, Zhang, L and Xu, J, 2019. Recovery and purification of metallic silicon from waste silicon slag in electromagnetic induction furnace by slag refining method. *Journal of Cleaner Production*, 229:1335–1341.